IEEE Access
Multidisciplinary | Rapid Review | Open Access Journal

Received 3 June 2022, accepted 21 June 2022, date of publication 27 June 2022, date of current version 1 July 2022.

Digital Object Identifier 10.1109/ACCESS.2022.3186281

RESEARCH ARTICLE

Mutual Transformation of Flux-Controlled and Charge-Controlled Memristors

DALIBOR BIOLEK[1,2], (Senior Member, IEEE), ZDENĚK KOHL[2], JIRI VAVRA[2], VIERA BIOLKOVÁ[3], (Member, IEEE), KAPIL BHARDWAJ[4], AND MAYANK SRIVASTAVA[4]

[1]Department of Microelectronics, Brno University of Technology, 616 00 Brno, Czech Republic
[2]Department of Electrical Engineering, University of Defence, 662 10 Brno, Czech Republic
[3]Department of Radio Electronics, Brno University of Technology, 616 00 Brno, Czech Republic
[4]Department of Electronics and Communication Engineering, National Institute of Technology Jamshedpur, Jamshedpur, Jharkhand 831014, India

Corresponding author: Dalibor Biolek (dalibor.biolek@unob.cz)

This work was supported in part by the Czech Science Foundation under Grant 20-26849S; and in part by the Project for the Development of the Organization, University of Defence Brno, Czech Republic.

ABSTRACT Two-ports for mutual transformation between flux-controlled memristors and charge-controlled memristors are proposed. Attention is paid to memristors with the region of negative differential memristance in the charge-flux constitutive relation, when such a transformation should be made carefully. Connections between this transformation, duality rules, and Chua's table of higher-order elements are described. The proposed transforming cells can be made up of commercially available integrated circuits. Their proper operation is demonstrated via simulations and lab experiments with memristive oscillators.

INDEX TERMS Charge-controlled memristor, flux-controlled memristor, higher-order element, constitutive relation, oscillator, gyrator, OTA, CCII.

I. INTRODUCTION

Today's resistive memory devices for non-volatile memories, memristive logic circuits or devices emulating neuromorphic systems are modelled as the so-called memristive systems [1], which are a generalization of the original concept of the memristor introduced in 1971 [2]. According to the current terminology, memristive systems are called extended memristors while the memristor from [1] is denoted as the ideal memristor [3]. In addition to the important role of memristors as models of existing memristive devices, the ideal or ideal generic memristors [3] are important building blocks of the so-called predictive modeling [4] whose key idea is to build complex nonlinear models of existing systems from a set of fundamental electrical elements, the ideal memristor being one of them.

The predictive model of the ideal memristor is its constitutive relation between the charge q and the flux φ, i.e. between the first time integrals of the memristor current and voltage [3]. The form of this relation predetermines the memristor behavior under arbitrary conditions. For passive memristors, the relation $\varphi = \widehat{\varphi}(q)$ is strictly monotonic, and the corresponding inversion leads to the equivalent relation $q = \widehat{q}(\varphi)$. However, if the monotonicity does not hold, then at least one of the above constitutive relations does not exist as one-to-one correspondence. Then, according to the terminology from nonlinear electrical systems [5], the memristor with the unambiguous relation $\varphi = \widehat{\varphi}(q)$ and ambiguous relation $q = \widehat{q}(\varphi)$ is called the charge-controlled memristor (QCM). The contrary case leads to the flux-controlled memristor (FCM).

The laboratory experiments with memristive circuits can be performed either with memristors as existing solid-state devices or with their hardware emulators. The first case is rather rare since there are only a few possibilities of purchasing memristors [6], and the behavior and parameters of these devices may not correspond well to memristors with parameters required for specific experiment. That is why the popular method is to develop and build various kinds of memristor emulators.

Anyway, it can be useful to provide the QCM-to-FCM conversion if the available memristor is of the QCM type,

The associate editor coordinating the review of this manuscript and approving it for publication was Baker Mohammad.

This work is licensed under a Creative Commons Attribution 4.0 License. For more information, see https://creativecommons.org/licenses/by/4.0/

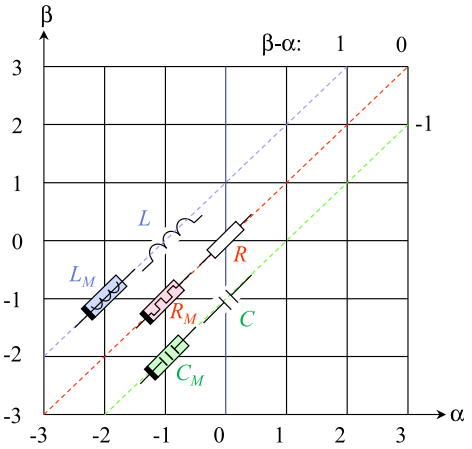

FIGURE 1. Fragment of Chua's table of higher-order elements. The α axis is associated with voltage and its derivatives (α positive) or integrals (α negative), the β axis with current and its derivatives (β positive) or integrals (β negative). The resistor (R), capacitor (C), inductor (L), memristor (R_M), memcapacitor (C_M), meminductor (L_M) have the coordinates (α, β) = (0, 0), (0, −1), (−1, 0), (−1, −1), (−1, −2), and (−2, −1), respectively.

and we request the FCM for a specific application. Similarly, analogous requests may appear for the FCM-to-QCM conversion. Such conversion circuits may be also interesting when the conversion is accompanied by modifying the shape of the original constitutive relation to the requested form. The simplest form of this shaping is the linear scaling.

The above conversion can be resolved by a combination of the concept of duality for memristors and higher-order elements [7] and the element transformation via gyrators [8].

The aim of this work is to present the circuit ideas of the FCM-to-QCM and QCM-to-FCM conversions. The duality and gyrator concepts are summarized in Section II. In Section III, the FCM-to-QCM and QCM-to-FCM converters are synthetized, with the conclusion that the latter is the same as the well-known OTA-based gyrator [9]. Suggested are implementations of these converters via off-the-shelf integrated circuits. Section IV demonstrates possible converter applications, computer simulations and laboratory experiments.

II. ELEMENT-TO-ELEMENT TRANSFORMATION IN CHUA'S TABLE

Fig. 1 demonstrates the position of selected six fundamental circuit elements in Chua's table. Each element is defined by its constitutive relation between a pair of the variables $(v^{(\alpha)}, i^{(\beta)})$, where $v^{(\alpha)}/i^{(\beta)}$ is the time derivative or integral of element voltage/current of order α/β if α/β is positive or negative [10]. The quantities $v^{(\alpha)}$ and $i^{(\beta)}$ are also referred to as generalized voltage and generalized current.

Let us consider an element with the coordinates (α, β) defined by the unambiguous constitutive relation

$$i^{(\beta)} = \widehat{i}^{(\beta)}(v^{(\alpha)}) \tag{1}$$

and with the ambiguous constitutive relation

$$v^{(\alpha)} = \widehat{v}^{(\alpha)}(i^{(\beta)}) \tag{2}$$

Then such element is the (α, β) element controlled by the generalized voltage $v^{(\alpha)}$, or, in short, the voltage-controlled (α, β) element.

It is obvious that also the $i^{(\beta)}$– controlled, or current-controlled (α, β) element with unambiguous constitutive relation (2) and ambiguous relation (1) can be defined accordingly.

According to this notation, the charge-controlled memristors (QCM) and flux-controlled memristors (FCM) can also be denoted as the current- and voltage- controlled memristors.

It follows from the concept of electrical duality [11] that the dual element can be generated from the original element by interchanging the voltage and current. That is why the voltage-controlled (α, β) element with the constitutive relation (1) has its dual element in the form of current-controlled (β, α) element with the constitutive relation

$$v^{(\beta)} = \widehat{v}^{(\beta)}(i^{(\alpha)}) \tag{3}$$

It should be noted that every (α, β) element from Chua's table has its dual representation located in the table on the coordinates (β, α), thus symmetrically to the position of the original element with respect to the diagonal with the parameter β–$\alpha = 0$, drawn in Fig. 1 in red. Then, for example, the dual element to the inductor is the capacitor. Concerning the elements located on the above diagonal, for example, the resistor is changed to the conductor after interchanging the voltage and current. However, the nature of the elements on this diagonal is not changed due to duality transformation. As a particular result, the QCM and the FCM are dual elements. That is why the QCM-to-FCM and FCM-to-QCM converters should provide the duality transformation. In general, such a transformation can be accomplished via the gyrator.

Consider the gyrator in Fig. 2 (a). Taking into account its gyration conductance G and the direction of the current i_2 chosen as in Fig. 2 (a), its classic equations [5] are rewritten as follows:

$$i_1 = Gv_2 \tag{4}$$
$$i_2 = Gv_1 \tag{5}$$

It is well-known that if the port 2 of the gyrator is connected to a current-controlled nonlinear resistor, then its port 1 behaves as a voltage-controlled resistor [5]. This observation can be generalized for the case of an arbitrary higher-order (α, α) element, i.e. an element located on the ''red'' diagonal in Chua's table in Fig. 1, connected to the port 2 as illustrated in Fig. 2 (b). Differentiating/integrating (4) and (5) α-times, $\alpha \in Z+/Z-$ yields the gyrator equations for generalized voltages and currents

$$i_1^{(\alpha)} = Gv_2^{(\alpha)} \tag{6}$$
$$i_2^{(\alpha)} = Gv_1^{(\alpha)} \tag{7}$$

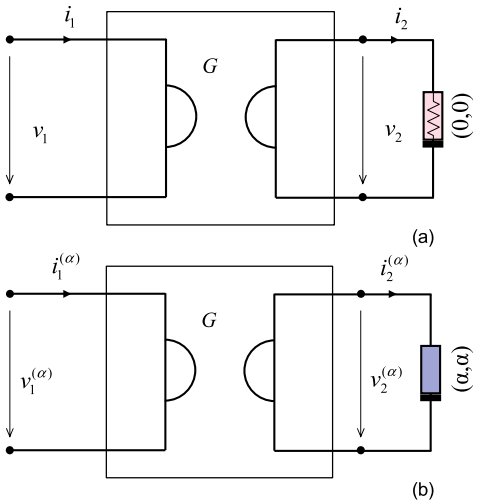

FIGURE 2. (a) Gyrator for transforming a nonlinear resistor connected to port 2 into a nonlinear conductor at port 1; (b) identical gyrator for transforming an arbitrary nonlinear (α, α) element located on the diagonal β–$\alpha = 0$ in Chua's table. The classic two-port current directions are intentionally modified in order to preserve the associated reference directions [5] of voltage and current of the element connected to port 2.

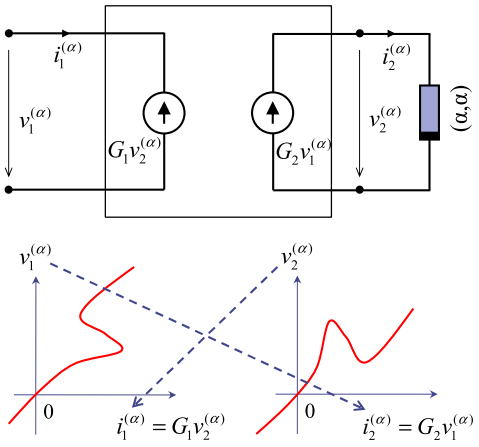

FIGURE 3. Procedure of the synthesis of a circuit that transforms a current-controlled (α, α) element into a voltage-controlled (α, α) element. For $\alpha = -1$, this circuit is the QCM-to-FCM converter.

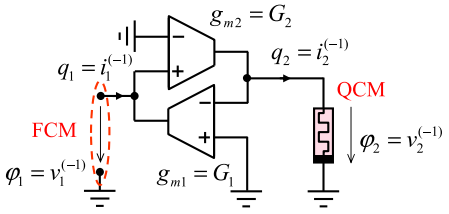

FIGURE 4. Implementation of the cell for QCM-to-FCM transformation via two gm stages.

It can be concluded from (6), (7) and from the corresponding Fig. 2 (b) that the classic gyrator can also be useful for transforming not only nonlinear controlled resistors but also an infinite number of other (α, α) elements, thus also memristors for $\alpha = -1$. It will be shown in the next Section that the particular implementation of the gyrator should be different for the FCM-to-QCM and QCM-to-FCM conversions. If the (α, α) element in Fig. 2 (b) is controlled by current, then it must be driven from the gyrator port 2 via a current source. It is in conformity with Eq. (7), which can be implemented as a transconductance amplifier with the transconductance G. In this particular case of converter, it can be therefore implemented via two OTAs (Operational Transconductance Amplifiers). However, if the (α, α) element being converted is controlled by voltage, then it requires voltage driving, and the gyrator equations should be rearranged in the form

$$v_2^{(\alpha)} = R i_1^{(\alpha)} \tag{8}$$

$$v_1^{(\alpha)} = R i_2^{(\alpha)} \tag{9}$$

where $R = 1/G$. Such a transforming cell should be implemented via two current-to-voltage converters.

It follows from the above analysis that the gyrator as a resistive two-port cannot be used for transforming between the voltage- controlled and current-controlled (α, β) elements for $\alpha \neq \beta$. Such transforming cells should contain blocks for time-domain integration or differentiation [12].

III. QCM-TO-FCM AND FCM-TO-QCM CONVERTERS

Consider a current-controlled nonlinear (α, α) element with the constitutive relation given on the right side of Fig. 3. The procedure of its conversion to a voltage-controlled (α, α) element with the left-side constitutive relation consists of the following steps:

1) Since the original element is controlled by current, it is driven by a current source that adjusts its proper operating point. The driving current is derived from the voltage of the transformed element through the proportionality factor G_2.
2) The generalized voltage at the operating point of the original element, which follows from the unambiguous constitutive relation, is transferred into the generalized current of the transformed element with the proportionality factor G_1.

It should be noted that the corresponding transforming cell in Fig. 3 can be considered a generalized gyrator described by Eqs. (6), (7), with two different gyration conductances G_1, G_2 for ports 1 and 2, respectively. In the case of emulating a grounded memristor, it can be implemented by the well-known circuit containing two OTAs in Fig. 4.

A similar procedure, summarized in Fig. 5, can be applied to the synthesis of the FCM-to-QCM converter. The voltage-controlled (α, α) element is driven by a voltage source controlled by a generalized current of the emulated element, with the proportionality factor R_2. The current flowing through the original element is sensed and used for controlling the voltage across the port 1 with the proportionality factor R_2. This way, the interchanging the voltage and current axes of the constitutive relations of both

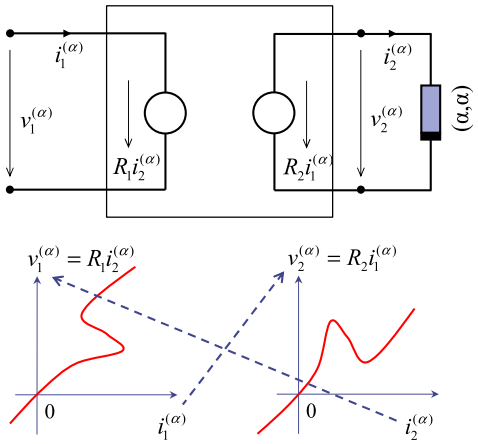

FIGURE 5. Procedure of the synthesis of a circuit which transforms a voltage-controlled (α, α) element into a current-controlled (α, α) element. For $\alpha = -1$, this circuit is the FCM-to-QCM converter.

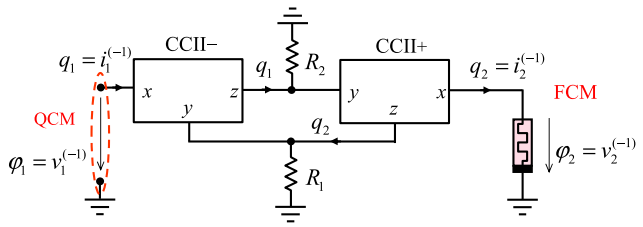

FIGURE 6. Implementation of the cell for FCM-to-QCM transformation via two current conveyors.

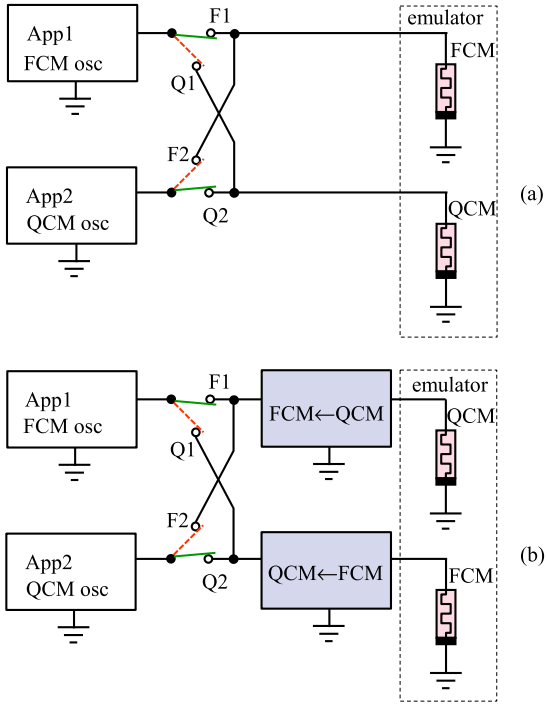

FIGURE 7. Experimental setup: (a) Verification without transforming cells: Application 1 (App1-memristive oscillator) works only with the FCM (switch position F1), application 2 (App2-dual oscillator) only with the QCM (switch position Q2); (b) Verification of transforming cells: App1/App2 works only in cooperation with the QCM-to-FCM/FCM-to-QCM converter (switch position F1/Q2).

elements applies. It is obvious that the transforming cell is a generalized gyrator described by Eqs. (8) and (9) with two different gyration resistances R_1 and R_2.

An implementation of the FCM-to-QCM converter via a pair of positive and negative current conveyors is proposed in Fig. 6. This converter can be easily implemented by means of off-the-shelf integrated circuits. The CCII+ is available as AD844 and the CCII- can be made of two CCII+. The low-impedance x terminal of the CCII+ drives the FCM while its (generalized) current is sensed and copied to the z terminal, which drives R_1. The corresponding voltage drop on R_1 is copied to the x terminal of the CCII- for driving the port 1. The current flowing through this port is then mirrored to the z terminal of the CCII-, causing the voltage across R_2. This voltage is then reflected directly to the port 2.

IV. EXPERIMENTAL VERIFICATION

Experimental verification of the idea of the FCM-to-QCM and QCM-to-FCM conversions can be given in the following steps: 1. Building FCM and QCM emulator pair with the constitutive relations providing negative differential memristances. 2. Finding two applications, the first (App1) working correctly only with the FCM, and the second (App2) only with the QCM. 3. Constructing two converters, the FCM-to-QCM and the QCM-to-FCM gyrators. 4. Proving that the App1 does not work with the QCM and works well with the QCM plus the QCM-to-FCM converter. 5. Proving that the App2 does not work with the FCM and works well with the FCM plus FCM-to-QCM converter. The experimental setup and a detail of the laboratory workplace are shown in Figs 7 and 8.

Before proceeding to laboratory measurements, the performance of designed circuits has been studied and verified via the SPICE simulations.

A. FCM AND QCM WITH NEGATIVE DIFFERENTIAL MEMRISTANCES

The memristors with non-monotonic constitutive relations can be easily implemented as popular and in the literature well described memristors with piece-wise-linear characteristics [3], [13]. Such locally active memristors can be useful for constructing nonlinear oscillators, artificial neurons, and networks working on the edge of chaos [14], [15], while passive memristors are useful for mimicking the synapses [16]. Emulators of the active memristors are used in this work for generating nonlinear oscillations via two benchmark circuits, denoted above as the applications App1 and App2. These memristive oscillators fall into the class of the oscillators introduced in [13] by Itoh and Chua.

The memristive emulators published so far can be classified as analog and hybrid [17], [18], the latter containing the analog memristive port, the analog-to-digital interface, and a part of digital signal processing. Since the analog emulators do not provide a flexible modification of the

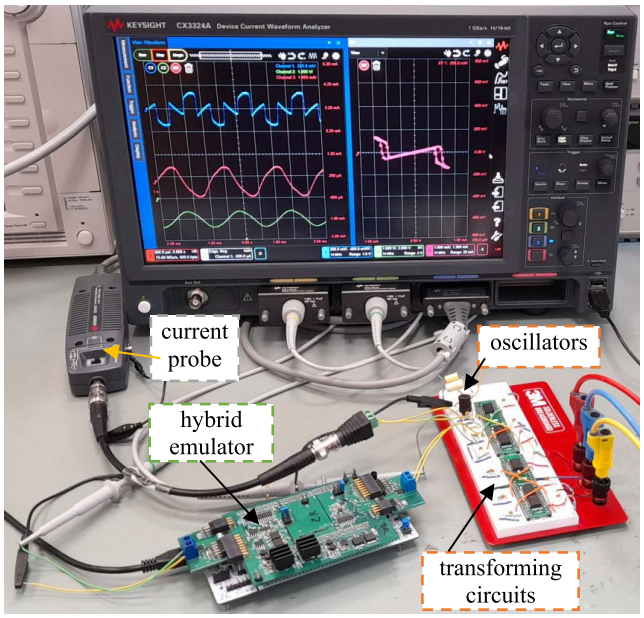

FIGURE 8. Laboratory workplace.

nonlinear characteristics of the emulated memristors, the hybrid approach was used.

The memristors with piece-wise-linear constitutive relations shown in Fig. 9 were simulated as current and voltage sources controlled by time integrals of the memristor voltage and current, respectively. For lab experiments, the memristors were emulated by the hybrid emulator described in [19]. In general, the memristive port can be emulated via one of three modules, namely the digital potentiometer (R-module), the controlled voltage source (V-module), and the controlled current source (I-module). These modules are controlled by a program according to the specific forms of the port and state equations of the emulated memristor.

Since the emulated memristors exhibit negative differential memristance, the R-module should be avoided. Finally, the FCM was emulated by the I-module and the QCM by the V-module according to Figs. 9 (a) and (b), respectively.

In addition to the maximum achievable sampling frequency of 100 kHz, there are also some voltage and current limitations associated with the V and I modules that must be taken into account, namely abs(v) $<$ 3 V and abs(i) $<$ 3 mA [19].

B. BENCHMARK CIRCUITS – NONLINEAR MEMRISTIVE OSCILLATORS

The circuit in Fig. 10 (a) can be considered a parallel combination of linear capacitor and the FCM with nonlinear flux-to-charge constitutive relation in Fig. 9 (a), driven via a pulse voltage source in series with a linear inductor L.

The corresponding dual circuit in Fig. 10 (b) forms the serial connection of the inductor and the QCM with nonlinear charge-to-flux constitutive relation in Fig. 9 (b), driven by a current pulse source in parallel with a linear capacitor.

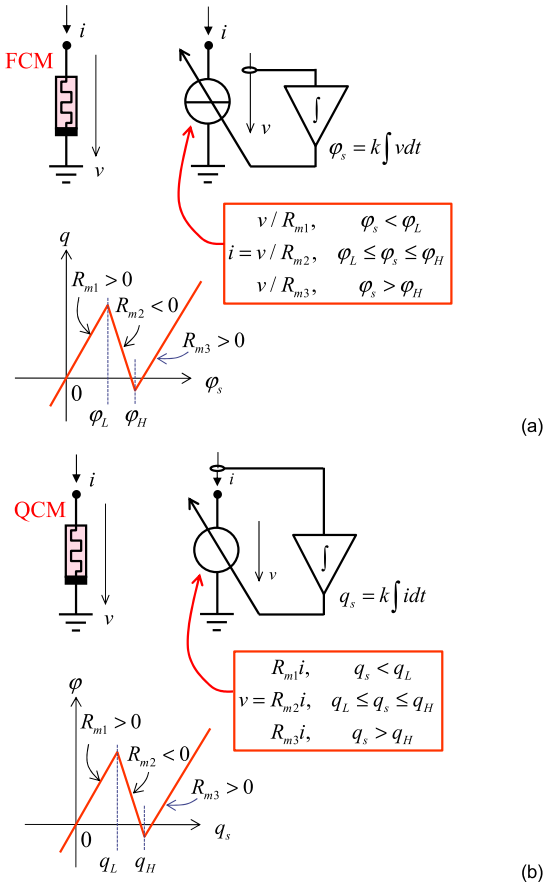

FIGURE 9. Implementation of the (a) FCM, (b) QCM with negative differential memristance by the hybrid emulator. φ_s and q_s are the flux and charge, scaled by a parameter k. Scaling is necessary to ensure a proper dynamic range of signals.

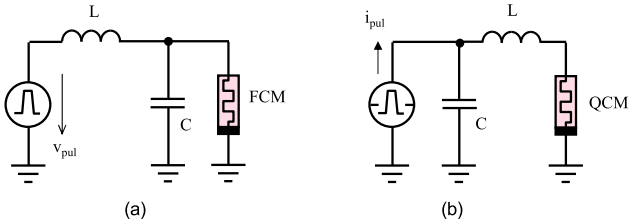

FIGURE 10. Dual oscillation circuits based on memristors with negative differential memristances of (a) FCM, (b) QCM types.

The circuit in Fig. 10 (a) resembles the well-known oscillator employing the tunnel diode, thus a voltage-controlled nonlinear resistor with negative differential resistance whose operating point is set into the region of negative resistance via a DC voltage source. The oscillator in Fig. 10 (a) uses the FCM instead of the tunnel diode. The operating point of the FCM is set via a pulse source v_{pul}. In fact, the circuit in Fig. 10 (a) is obtained from this classic circuit via applying the so-called "shift-type" duality transformation, where the nonlinear resistors are transformed into memristors, the voltage sources are replaced by flux sources, while the linear elements are preserved [20]. Then the strength of the narrow

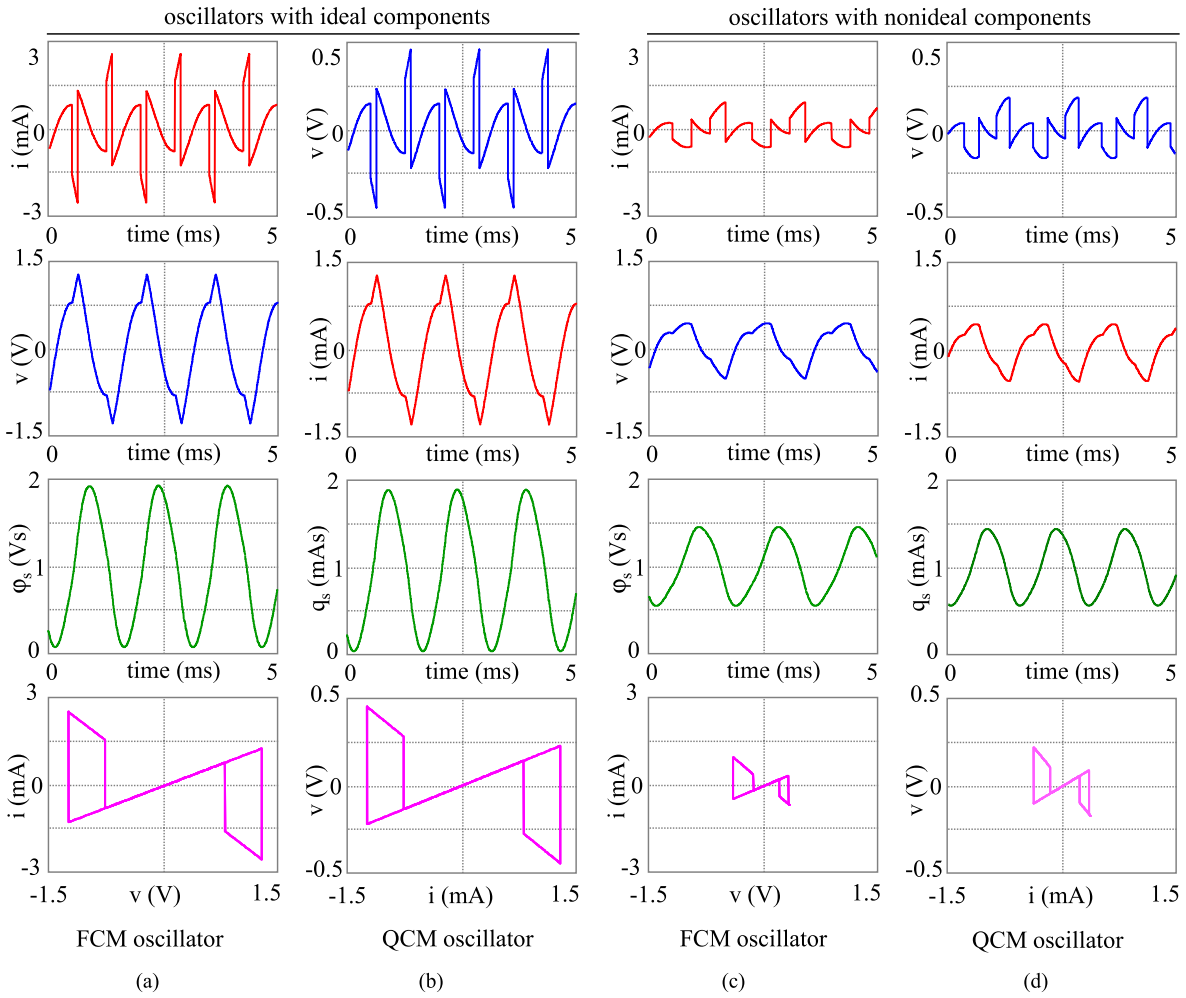

FIGURE 11. Transient analysis of the memristive oscillators from Figs. 10 (a), (b) employing the FCM and QCM. The quantities i, v, φ_s and q_s are the memristor current, voltage, and scaled flux and charge.

pulse v_{pul} should correspond to the voltage of the original DC source. The purpose of this pulse is to deliver the flux to the memristor, which moves its operating point into the region of its negative memristance.

The oscillations in the dual circuit in Fig. 10 (b) are initiated by a pulse from the current source i_{pul}. The amount of the corresponding charge injected into the circuit moves the operating point of the QCM into the interval q_L, q_H of the flux-charge constitutive relation of the QCM in Fig. 9 (b).

The technical limits of the emulator have been taken into account when designing the oscillator parameters. Since the sampling frequency used by the digital part of the emulator is 100 kHz, the oscillation frequency should be designed below 1 kHz, thus eliminating the accuracy issue caused by a limited number of samples within one repeating period. A low oscillating frequency leads to large inductance with high ESR (Equivalent Series Resistance), the latter affecting the oscillating frequency and potentially damping the oscillation. The impedance level, i.e. the oscillator reactances at given frequency and the emulator memristances, should be also designed with regard to the current and voltage limits associated with the V- and I- modules of the emulator.

Oscillators in Fig. 10 were designed with the following parameters:

$L = 100$ mH, $C = 560$ nF,

FCM: $a = 3826$, $\varphi_L = 0.75$ Vs, $\varphi_H = 1.25$ Vs, $R_{m1} = R_{m3} = 1$ kΩ, $R_{m2} = -500$ Ω, v_{pul}: 1 V/261 μs

QCM: $a = 3826$, $q_L = 0.75$ mAs, $q_H = 1.25$ mAs, $R_{m1} = R_{m3} = 178.5$ Ω, $R_{m2} = -357$ Ω, i_{pul}: 1 mA/261 μs.

Note that the oscillator in Fig. 10 (b) was designed from the oscillator in Fig. 10 (a) as a dual circuit, applying the following voltage and current scaling that optimize the dynamic range of voltages and currents:

$$i' = k_i v,\ k_i = 1\ \text{mS}, \tag{10}$$

$$v' = k_v i,\ k_v = 178.6\ \Omega, \tag{11}$$

where v, i/v', i' are the voltages and currents of the original/dual circuit, and k_i and k_v are scaling coefficients. Then, according to the well-known duality rules, the resistor

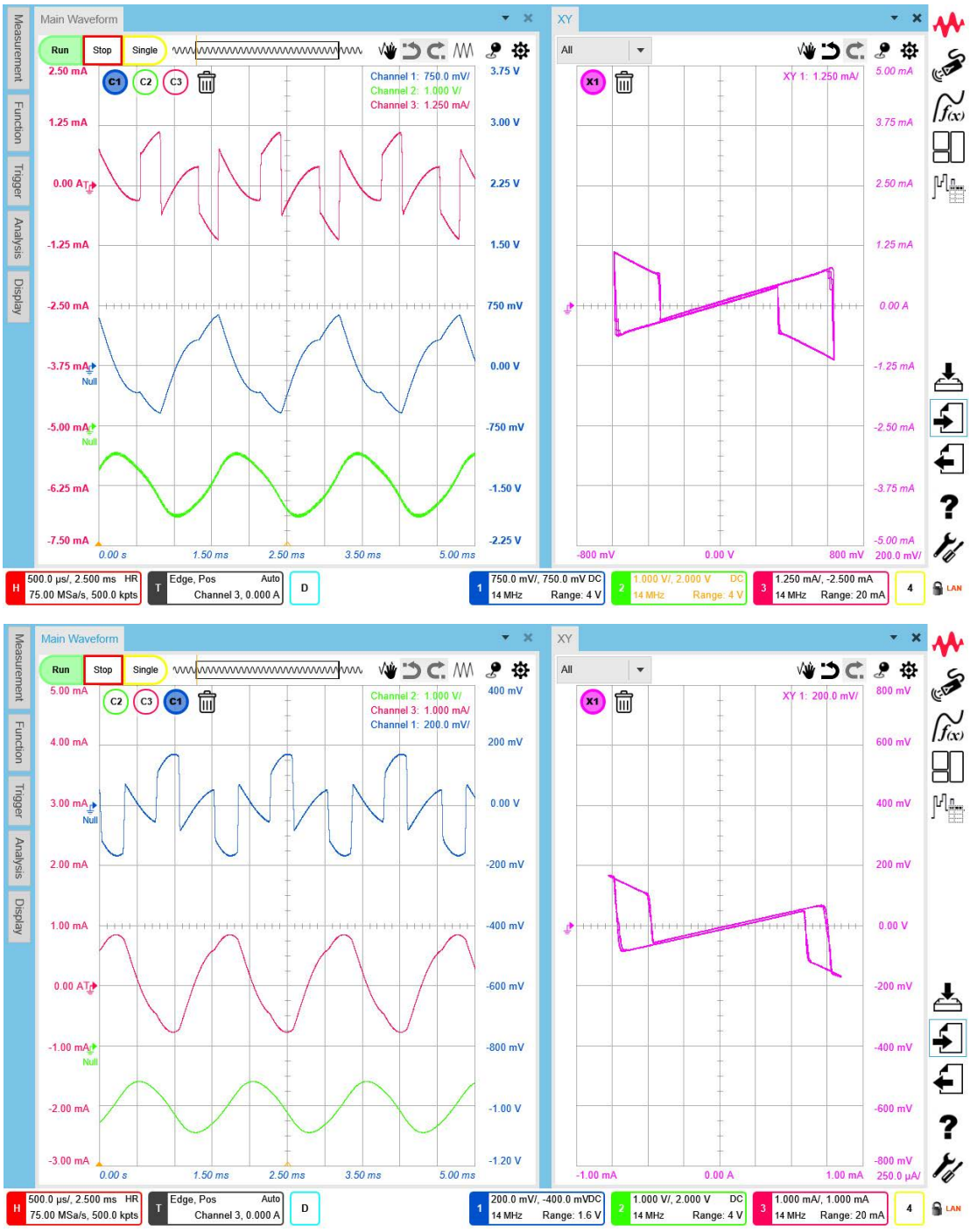

FIGURE 12. **Measured memristor waveforms in a top-down order: FCM oscillator (upper section: current, voltage, flux), QCM oscillator (bottom section: voltage, current, charge).**

R is changed to conductor $G' = Rk_i/k_v$, the inductor L to capacitor $C' = Lk_i/k_v$, and the capacitor C to inductor $L' = Ck_v/k_i$.

After applying the above transformations, the oscillators in Figs. 10 (a), (b) have dual properties, so their oscillation frequencies should be the same. The results of the SPICE simulations in Figs. 11 (a), (b) for the designed parameters of ideal components confirm dual waveforms with an oscillation frequency of ca 665 Hz.

The simulations also confirm the hypothesis that the oscillations can be accomplished without the triggering pulses via setting proper initial values of the memristor state. For the oscillators in Figs. 10 (a) and (b), the initial scaled flux and charge should be set to 1 Vs and 1 mAs, respectively.

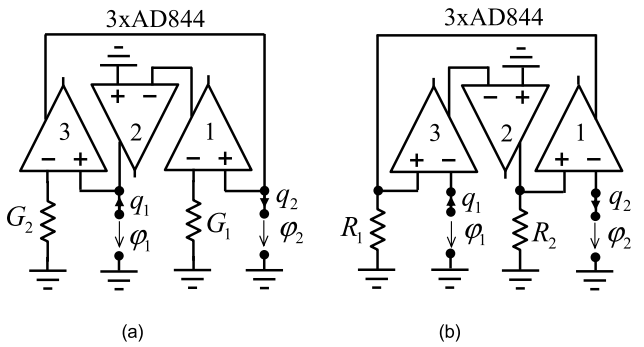

FIGURE 13. Implementation of (a) QCM-to-FCM, (b) FCM-to-QCM converter via 3 × AD844.

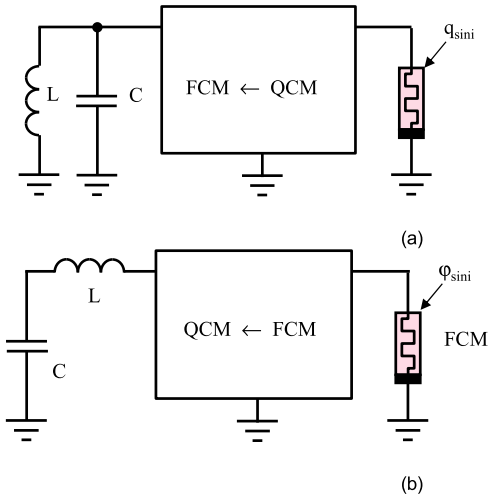

FIGURE 14. Dual oscillation circuits based on memristors with negative differential memristances of (a) FCM, (b) QCM types. To prove the proper operation of conversion circuits, the FCM (QCM) is implemented by a hybrid emulator of the QCM (FCM) and the QCM-to-FCM (FCM-to-QCM) converter. The oscillation is accomplished via setting a proper initial value of memristor state.

It reduces the above oscillating circuits to three elements in parallel and in series.

Figs. 11 (c), (d) demonstrate the oscillator sensitivity to parasitic losses in the circuit, namely to the serial resistance R_L of the inductor. This effect is clearly visible for rather high resistance $R_L = 200\ \Omega$ which is comparable to the memristances R_{m1}, R_{m2}, and R_{m3}, in decreasing levels and modified shapes of the generated waveforms. It is also evident that the operating point of the memristor is slightly moved from the center of the region of negative memristance, which causes an asymmetry in the $v - i$ pinched hysteresis loops. It is worth noting that such parasitic effects also disturb the waveform duality.

Finally, the oscillators from Figs. 10 (a), (b) were constructed via the hybrid emulators of the FCM and QCM with the parameters given in Section B. The oscillations were provided by setting the initial values of $q_{sini} = 1$ mAs and $\varphi_{sini} = 1$ Vs. Special attention was paid to the algorithm of numerical integration of the memristor voltage and current in order to compute their state variables. The simple Euler method amplifies undesired low-frequency fluctuations and, concurrently, it does not provide an exact phase shift of 90 degrees, which is necessary for a proper generation of $v - i$ pinched hysteresis loops of memristors. The best results were achieved with a lossy bilinear integrator with a cutoff frequency of 10 Hz.

Fig. 12 shows the waveforms and pinched hysteresis loops generated by specimens of the oscillators. The initial conditions were slightly modified in order to achieve symmetric hysteresis. The measurements are in good agreement with SPICE simulations.

C. QCM-TO-FCM AND FCM-TO-QCM CONVERTERS

The QCM-to-FCM converter in Fig. 4 is based on two OTAs. Since the commercial OTAs such as LM13700 provide low input resistance and also low range of input voltage for linear operation, this converter was finally implemented by three AD844 transimpedance amplifiers as shown in Fig. 13 (a). The amplifier No. 1 together with G_1 form a transconductance amplifier with the transconductance G_1. The amplifier No. 2 serves as the current inverter for driving the port No. 1 whereas the amplifier No. 3, whose high-impedance input is driven also from the port No. 1, operates as OTA with the transconductance G_2. Its high-impedance output drives the port No. 2.

Since the voltage outputs of the amplifiers No. 1 and 3 provide buffered signals appearing on inverting inputs, they can be used for sensing the voltages across the ports No. 2 and 1, respectively.

The implementation of the FCM-to-QCM converter from Fig. 6 via three transimpedance amplifiers is shown in Fig. 13 (b). The schematics is similar to the QCM-to-FCM converter in Fig. 13 (a), but now, the amplifiers play the role of current conveyors according to Fig. 6. The amplifier No. 1 forms the conveyor CCII+ whereas the amplifiers 3 and 2 work as the CCII-.

D. MEMRISTIVE OSCILLATORS WITH QCM-TO-FCM AND FCM-TO-QCM CONVERTERS

In order to check the idea of the QCM-to-FCM and the FCM-to-QCM conversions via circuits from Figs. 4 and 6, SPICE simulations and laboratory experiments were accomplished according to Figs. 14 (a) and (b).

As expected, the parallel LC cell in Fig. 14 (a) provided the autonomous oscillations with the FCM but not with the QCM, and the serial LC cell in Fig. 14 (b) worked well with the QCM but not with the FCM. In other words, the circuits in Fig. 13 cannot oscillate after removing the converters from the networks. The parallel configuration can oscillate with the memristor of the N-type flux-to-charge characteristic, and the series configuration with the memristor of the N-type charge-to-flux characteristic.

For experiments, the SPICE models and specimens of the conversion circuits from Fig. 13 were constructed. Since the converters form an interface between the original and dual

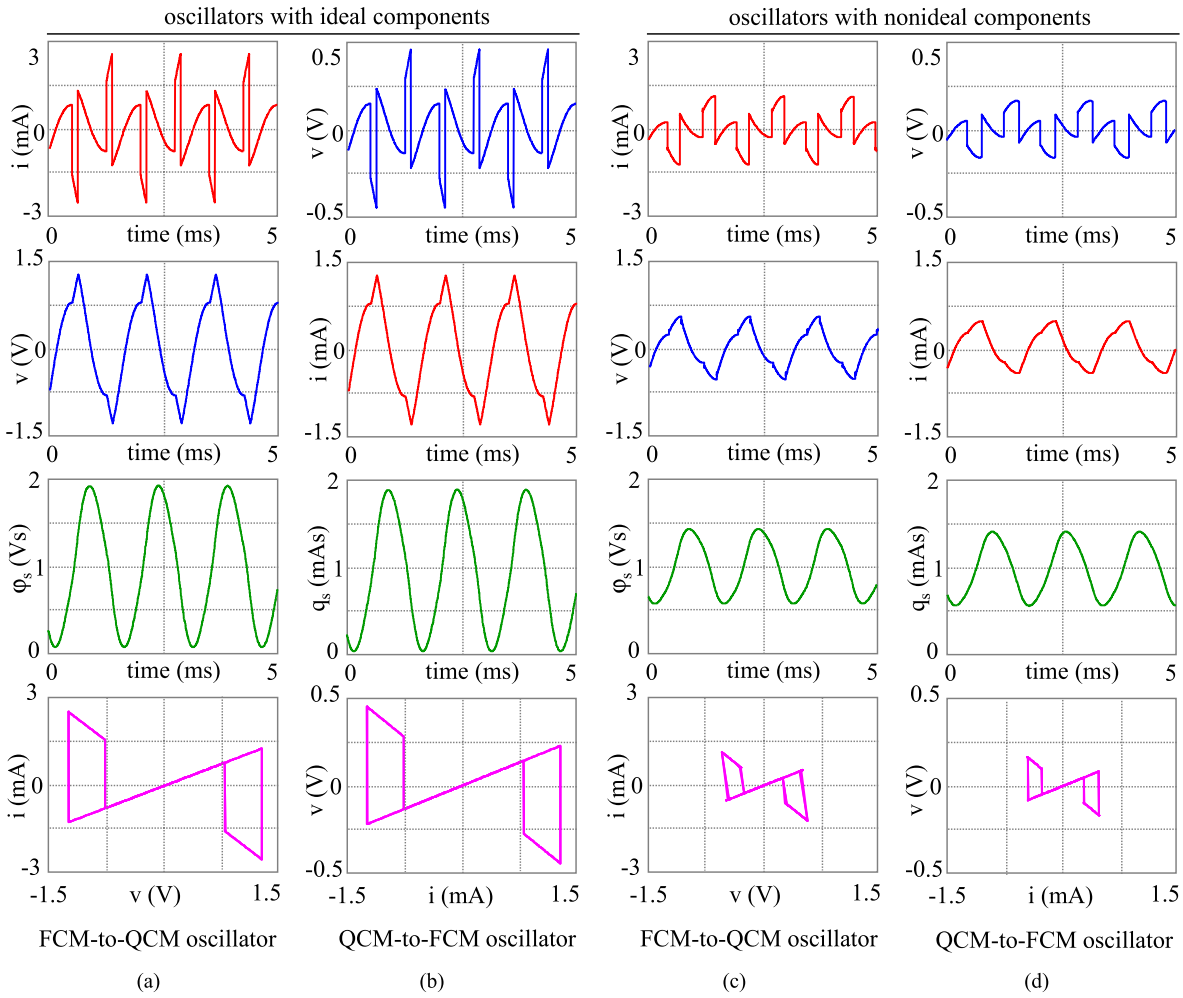

FIGURE 15. **Transient analysis of the memristive oscillators from Fig. 14. The waveforms in Figs. (c), (d) are simulated for the conversion circuits employing the AD844 and for $R_L = 150\ \Omega$.**

circuitry, their transforming port equations should be in the form of Eqs. (10), (11). That is why the resistances $1/G_1$ and $1/G_2$ in the QCM-to-FCM converter and the resistances R_1 and R_2 in the FCM-to-QCM converter in Fig. 13 were designed as $1/G_1 = R_1 = k_v = 178.6\ \Omega$, $1/G_2 = R_2 = 1/k_i = 1\text{k}\Omega$.

In addition to simple behavioral SPICE models based on ideal conversion equations between voltages and currents, the converters from Figs. 13 (a), (b) were also modeled with full SPICE model of AD844 and for various values of the lossy resistance of the inductor. A selection of the simulated waveforms is given in Figs. 15 (a), (b) (ideal components) and Figs. 15 (c), (d) (more complex modeling). Figs. 15 (a), (b) confirm the correctness of the idea of the conversion circuits. Simulations with non-ideal components reveal two main sources of imperfections, the parasitic resistances of the inverting inputs of the AD844 ($R_{AD} \approx 50\ \Omega$), and the above analyzed R_L. Figs. 15 (c) and (d) were drawn for $R_L = 150\ \Omega$. For this value, the simulated waveforms correspond well with the laboratory measurements given below in Fig. 16.

The mechanism of how R_{AD} affects the oscillator behavior is different for the QCM-to-FCM and for the FCM-to-QCM converters.

Observing the QCM-to-FCM implementation in Fig. 13 (a), it is obvious that the input resistances R_{AD} of the integrated circuits No. 1 and 3 act in series with $R_1 = 1/G_1$ and $R_2 = 1/G_2$. Then the corresponding scaling coefficients k_v and k_i, which determine the impedance transformations, are changed. This results in modifying the impedance conditions in the circuit.

For the FCM-to-QCM converter in Fig. 13 (b), these coefficients are not affected, but the R_{AD} now operates in series with both converter ports. As the negative consequence for the oscillator in Fig. 14 (b), R_{AD} is added to the lossy resistor R_L and also to the memristance of the FCM, thus increasing their values. Since the R_{AD} is rather high, it affects the memristor voltage and current waveforms as shown in Figs. 15 (c), (d).

The $v - i$ pinched hysteresis loop of the FCM in the FCM-to-QCM oscillator exhibits a specific "sloping distortion". An analysis reveals that the cause consists in the

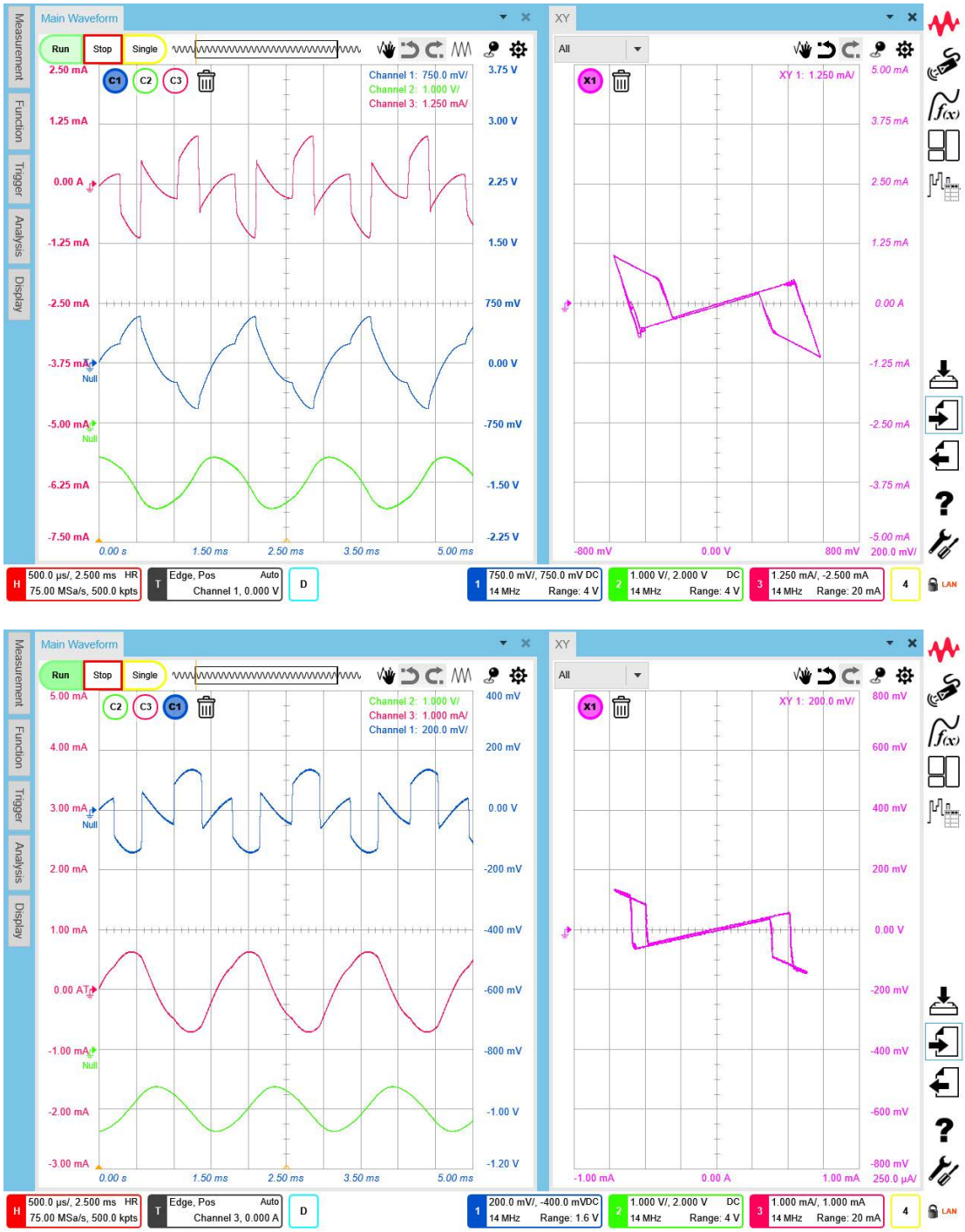

FIGURE 16. Measured memristor waveforms in the top-down order: FCM-to-QCM oscillator (upper section: current, voltage, flux), QCM-to-FCM oscillator (bottom section: voltage, current, charge).

voltage drop on the R_{AD} which operates in series with the memristor. The experiments with the SPICE model also demonstrate a high sensitivity of the shapes of generated signals to the initial state of the memristor (the initial charge of the QCM and the initial flux of the FCM). For example, the waveforms of the QCM-to-FCM oscillator in Fig. 15 (d) were obtained with an initial charge of 1.07 mAs. For the standard value of 1 mAs, the hysteresis lobes were strongly asymmetric, because the mean value of the charge waveform was shifted down due to changing the impedance conditions in the circuit.

The measurements confirmed the above error analysis. The waveforms from Fig. 16 were obtained after fine-tuning the initial conditions q_{ini} and φ_{ini}.

Although it may be beyond the main idea of this article, it is worth mentioning that the negative effects of parasitic resistances on the oscillator behavior can be partially compensated by modifying the resistances acting in series, namely the resistors in transforming circuits and the memristor resistances R_{m1}, R_{m2}, and R_{m3}.

V. CONCLUSION

The results presented in this work can be summarized as follows:

1. The demand for the charge-controlled memristor when only its flux-controlled counterpart is available and vice versa can be settled by simple transforming two-ports.
2. If a flux-controlled memristor with unambiguous flux-to-charge characteristic and ambiguous charge-to-flux characteristic needs to be converted into a charge-controlled memristor, then the transforming cell is a resistive two-port consisting of two current-controlled voltage sources. It can be implemented via commercial current conveyors.
3. If a charge-controlled memristor with unambiguous charge-to-flux characteristic and ambiguous flux-to-charge characteristic needs to be converted into a flux-controlled memristor, then the transforming cell is a resistive two-port consisting of two voltage-controlled current sources. It can be implemented via commercial operational transconductance amplifiers (OTAs).
4. The two-ports from Items 2 and 3 can also be used for mutual conversions between the voltage-controlled and current-controlled nonlinear (α, α) higher-order elements from Chua's table, whose special case for $\alpha = -1$ is just the memristor.
5. The transforming cells from Items 2 and 3 provide the duality transformation. That is why the QCM-to-FCM converter can be generally used for the conversion from nonlinear current-controlled (α, β) element into nonlinear voltage-controlled (β, α) element, and the FCM-to-QCM converter from voltage-controlled (α, β) element into current-controlled (β, α) element. The well-known synthetic inductors based on a capacitor-to-inductor conversion are mere examples of these general converters.

The authors believe that the above converters may also become useful for re-shaping the nonlinear characteristics of memristive devices, which may appear on the market as solid-state devices with rigid nonlinearities.

The experiments with autonomous dual circuits containing memristors with negative differential memristances reveal several challenges that are worth studying in the future, for example the rules of changing the waveforms generated by a network whose topology is changed due to the duality rules, the mechanism of starting-up and stabilizing oscillations in memristive networks, or the stability of analog networks containing digital emulators.

REFERENCES

[1] L. O. Chua and S. M. Kang, "Memristive devices and systems," *Proc. IEEE*, vol. 64, no. 2, pp. 209–223, Feb. 1976.
[2] L. Chua, "Memristor—The missing circuit element," *IEEE Trans. Circuit Theory*, vol. IT-18, no. 5, pp. 507–519, Sep. 1971.
[3] L. Chua, "Everything you wish to know about memristors but are afraid to ask," *Radioengineering*, vol. 24, no. 2, pp. 319–368, 2014.
[4] L. Chua, "Device modeling via nonlinear circuit elements," *IEEE Trans. Circuits Syst.*, vol. CS-27, no. 11, pp. 1014–1044, Nov. 1980.
[5] L. O. Chua, C. A. Desoer, and E. S. Kuh, *Linear and Nonlinear Circuits*. New York, NY, USA: McGraw-Hill, 1987.
[6] *Memristors to Machine Intelligence*. Accessed: Jun. 15, 2022. [Online]. Available: https://knowm.org/
[7] D. Biolek, Z. Biolek, and V. Biolková, "Duality of complex systems built from higher-order elements," *Complexity*, vol. 2018, pp. 1–15, Nov. 2018.
[8] B. D. Tellegen, "The gyrator, a new electric network element," *Philips Res. Lab.*, vol. 3, no. 2, pp. 81–101, 1948.
[9] M. Bialko and R. Newcomb, "Generation of all finite linear circuits using the integrated DVCCS," *IEEE Trans. Circuit Theory*, vol. CT-18, no. 6, pp. 733–736, Nov. 1971.
[10] D. Biolek and Z. Biolek, "About fingerprints of Chua's memristors," *IEEE Circuits Syst. Mag.*, vol. 18, no. 2, pp. 35–47, May 2018.
[11] T. E. Stern, *Theory of Nonlinear Networks and Systems*. Reading, MA, USA: Addison-Wesley, 1965.
[12] D. Biolek, V. Biolková, and Z. Kolka, "Mutators simulating memcapacitors and meminductors," in *Proc. IEEE Asia Pacific Conf. Circuits Syst.*, Dec. 2010, pp. 800–803.
[13] M. Itoh and L. O. Chua, "Memristor oscillators," *Int. J. Bifurcation Chaos*, vol. 18, no. 11, pp. 3183–3206, 2008.
[14] L. Chua, "Memristors, Hodgkin-Huxley, and edge of chaos," *Nanotechnology*, vol. 24, Sep. 2013, Art. no. 383001.
[15] A. Ascoli, A. S. Demirkol, R. Tetzlaff, S. Slesazeck, T. Mikolajick, and L. O. Chua, "On local activity and edge of chaos in a NaMLab memristor," *Frontiers Neurosci.*, vol. 15, pp. 1–30, Apr. 2021.
[16] J. Sun, J. Han, Y. Wang, and P. Liu, "Memristor-based neural network circuit of emotion congruent memory with mental fatigue and emotion inhibition," *IEEE Trans. Biomed. Circuits Syst.*, vol. 15, no. 3, pp. 606–616, Jun. 2021.
[17] D. Biolek, "Memristor emulators," in *Handbook of Memristor Networks*. Cham, Switzerland: Springer, 2019.
[18] A. G. Alharbi and M. H. Chowdhury, *Memristor Emulator Circuits*. Cham, Switzerland: Springer, 2021.
[19] Z. Kolka, J. Vavra, V. Biolkova, A. Ascoli, R. Tetzlaff, and D. Biolek, "Programmable emulator of genuinely floating memristive switching devices," in *Proc. 26th IEEE Int. Conf. Electron., Circuits Syst. (ICECS)*, Nov. 2019, pp. 217–220.
[20] D. Biolek, J. Vavra, Z. Biolek, Z. Kolka, V. Biolkova, and J. Dobes, "Chua's table as a tool for constructing dual networks," in *Proc. IEEE Asia Pacific Conf. Circuits Syst. (APCCAS)*, Nov. 2019, pp. 145–148.

DALIBOR BIOLEK (Senior Member, IEEE) received the M.S. degree in electrical engineering from the Brno University of Technology (BUT), Czech Republic, in 1983, and the Ph.D. degree in electronics from the Military Academy Brno, Czech Republic, in 1989.

He is currently with the Department of EE, University of Defence Brno (UDB), and the Department of Microelectronics, BUT. He is also a Professor in the field of theoretical electrical engineering with BUT and UDB. His research interests include the areas of general circuit theory, frequency filters, mem-systems, and computer simulation of electronic systems.

Prof. Biolek is a member of the CAS/COM Czech National Group of IEEE. He has been a member of editorial boards of international journals, including the *International Journal of Electronics and Communications* (AEU) and *Electronics Letters*.

ZDENĚK KOHL received the M.S. degree in electrical engineering and the Ph.D. degree in electronics from the Brno University of Technology (BUT), Czech Republic, in 1982 and 1986, respectively.

He was worked with the Department of Radio Electronics, BUT, as an Assistant Professor, and shortly with the University Colorado of Boulder dealing with spectrum estimation. Later, he spent several years with Hewlett-Packard as a Technical Solutions Consultant. He is currently with the Department of Electrical Engineering, University of Defence Brno, Czech Republic. His research interests include digital signal processing, spectral analysis, and MCU usage for electronic elements emulation.

JIRI VAVRA received the M.S. and Ph.D. degrees from the Faculty of Electrical Engineering and Communication, Brno University of Technology, Czech Republic, in 2007 and 2012, respectively. He is currently an Associate Professor with the Department of Electrical Engineering, University of Defence, Brno, Czech Republic. His research interests include the area of analog signal processing, especially to current-mode circuits, frequency filters, and mem-systems.

VIERA BIOLKOVÁ (Member, IEEE) received the M.S. degree in electrical engineering from the Brno University of Technology, Czech Republic, in 1983. She joined the Department of Radio Electronics, in 1985. She is currently working as a Research Assistant with the Department of Radio Electronics, Brno University of Technology. Her research and educational interests include signal theory, analog signal processing, memristors and memristive systems, optoelectronics, and digital electronics.

KAPIL BHARDWAJ is currently a Research Scientist with NIT Jamshedpur, Jharkhand, India. He has authored and coauthored more than 25 research papers in reputed journals and international conferences. His research interests include analog integrated circuits, CMOS architectures, memristor realizations, and emulation of memristors and their applications in analog signal processing.

MAYANK SRIVASTAVA is currently working as an Assistant Professor with the Department of Electronics and Communication Engineering, NIT Jamshedpur, Jharkhand, India. He has authored or coauthored more than 60 research papers in international journals and conferences. His research interests include the areas of bipolar and CMOS analog integrated circuits and current-mode signal processing.